Supporting Information: Fluorinated Garnet: Benchmarking Li-Ion Conductivity Through Structure–Transport Correlations and Trade-Offs

Saumya Ranjan Mahanta and Swastika Banerjee*

Department of Chemistry, Indian Institute of Technology Roorkee, India

E-mail: sbanerjee@cy.iitr.ac.in

Computational Details

Energy Above Hull (E_{hull})

All first-principles calculations were performed using the Vienna *Ab initio* Simulation Package (VASP) within the framework of density functional theory (DFT). The exchange–correlation interactions were treated using the PBEsol functional, and the plane-wave basis set was expanded with an energy cutoff of 520 eV. The same k-point density was used consistently for all systems studied. Electronic energy convergence was achieved when the total energy difference between successive ionic steps was less than 1×10^{-5} eV.

The formation energy (E_{form}) of LLZO and the engineered LLZO systems was calculated relative to their most stable decomposition products according to:

$$E_{\text{form}} = \frac{E_{\text{compound}} - \frac{1}{a}\sum_i b_i E_i}{N_{\text{atoms}}} \tag{1}$$

where E_{compound} is the total DFT energy of the compound, E_i is the energy of the i^{th} decomposition product, b_i is its stoichiometric coefficient in the balanced decomposition reaction, a is the number of formula units of the reactant, and N_{atoms} is the total number of atoms in one formula unit of the reactant. A positive E_{form} indicates that the compound lies above the convex hull (metastable), while a negative value suggests thermodynamic stability against decomposition.

For example, the formation reaction of LLZO was written as:

$$2\,\text{Li}_7\text{La}_3\text{Zr}_2\text{O}_{12} \rightarrow 2\,\text{Li}_6\text{Zr}_2\text{O}_7 + \text{Li}_2\text{O} + 3\,\text{La}_2\text{O}_3 \tag{2}$$

The formation free energy (E_f) was defined as the difference between the total free energy of the target compound and the sum of free energies of its most stable decomposition

products. For LLZO, the expression is given as:

$$E_f = F_{\mathrm{Li_7La_3Zr_2O_{12}}} - F_{\mathrm{Li_6Zr_2O_7}} - \tfrac{1}{2}F_{\mathrm{Li_2O}} - \tfrac{3}{2}F_{\mathrm{La_2O_3}}. \tag{3}$$

In this case, the DFT energies of all reactants and products were used in the above equation to calculate E_{form} per atom.

CSDM Analysis

To quantitatively assess the degree of cubic symmetry, we introduce the **Cubic Symmetry Deviation Metric (CSDM)**, which captures the structural deviation from perfect cubic symmetry by accounting for both lattice parameters and interaxial angles. Both the atomic positions and the lattice parameters (cell shape and volume) were fully optimized prior to performing the CSDM analysis.

$$\text{Average lattice constant } (\bar{x}) = \frac{a+b+c}{3}$$

$$\text{Average angle } (\bar{\angle x}) = \frac{\alpha+\beta+\gamma}{3}$$

Lattice Constant Deviations:

$$\text{Deviation for } a = \left|\frac{a-\bar{x}}{\bar{x}}\right| \times 100$$

$$\text{Deviation for } b = \left|\frac{b-\bar{x}}{\bar{x}}\right| \times 100$$

$$\text{Deviation for } c = \left|\frac{c-\bar{x}}{\bar{x}}\right| \times 100$$

$$\text{Average lattice deviation} = \frac{\text{Deviation for } a + \text{Deviation for } b + \text{Deviation for } c}{3}$$

Angle Deviations:

$$\text{Deviation for } \alpha = \left| \frac{\alpha - \bar{\angle} x}{\bar{\angle} x} \right| \times 100$$

$$\text{Deviation for } \beta = \left| \frac{\beta - \bar{\angle} x}{\bar{\angle} x} \right| \times 100$$

$$\text{Deviation for } \gamma = \left| \frac{\gamma - \bar{\angle} x}{\bar{\angle} x} \right| \times 100$$

$$\text{Average angle deviation} = \frac{\text{Deviation for } \alpha + \text{Deviation for } \beta + \text{Deviation for } \gamma}{3}$$

Cubic Symmetry Deviation Metric (CSDM):

$$\text{CSDM} = \text{Average lattice deviation} + \text{Average angle deviation}$$

A lower CSDM value indicates a structure that is closer to ideal cubic symmetry. For a perfectly cubic structure, CSDM = 0.

Table S1: Computed formation free energy (E_{form}, meV/atom) and thermodynamically competing phases for pristine and modified LLZO compositions, as determined from DFT calculations employing the PBEsol exchange–correlation functional.

Composition	**Competing Phases**	E_{form} **(meV/atom)**
$\mathbf{Li_7La_3Zr_2O_{12}}$	$Li_6Zr_2O_7 + Li_2O + La_2O_3$	3
$\mathbf{Li_{6.25}AlLa_3Zr_2O_{12}}$	$Li_6Zr_2O_7 + LiAlO_2 + La_2O_3$	4
$\mathbf{Li_{6.25}GaLa_3Zr_2O_{12}}$	$Li_6Zr_2O_7 + LiGaO_2 + La_2O_3$	6
$\mathbf{Li_{5.5}AlGaLa_3Zr_2O_{12}}$	$Li_7La_3Zr_2O_{12} + La_2Zr_2O_7 + LiAlO_2 + LiGaO_2 + La_2O_3$	5
$\mathbf{Li_{5.5}Ga_2La_3Zr_2O_{12}}$	$La_2Zr_2O_7 + Li_6Zr_2O_7 + LiGaO_2 + La_2O_3$	16
$\mathbf{Li_{5.5}AlLa_3Zr_2O_{11.25}F_{0.75}}$	$La_2Zr_2O_7 + Li_6Zr_2O_7 + LiAlO_2 + LiF + La_2O_3$	20
$\mathbf{Li_{5.25}AlLa_3Zr_2O_{11}F}$	$La_2Zr_2O_7 + Li_6Zr_2O_7 + LiAlO_2 + LiF + La_2O_3$	24
$\mathbf{Li_{6.5}La_3Zr_2O_{11.5}F_{0.5}}$	$Li_6Zr_2O_7 + LiF + La_2O_3$	8
$\mathbf{Li_{6.25}La_3Zr_2O_{11.25}F_{0.75}}$	$Li_7La_3Zr_2O_{12} + La_2Zr_2O_7 + LiF + La_2O_3$	11
$\mathbf{Li_6La_3Zr_2O_{11}F}$	$Li_6Zr_2O_7 + La_2Zr_2O_7 + LiF + La_2O_3$	21

Table S2: Calculated Cubic Symmetry Deviation Metric (CSDM), which quantitatively evaluates deviations from ideal cubic symmetry by incorporating variations in both lattice parameters and interaxial angles. The structural data were obtained from NPT molecular dynamics simulations performed at 300 K for 10 ps.

System	**CSDM (%)**
LLZO	1.64
Al-LLZO	1.20
Ga-LLZO	1.22
Al-Ga-LLZO	0.46
Ga2-LLZO	0.78
Al-F4-LLZO	1.40
Al-F3-LLZO	0.98
F3-LLZO	0.71

Table S3: Summary of Li-ion migration barrier (E_{a}), extrapolated diffusion coefficient (D_0), and extrapolated room-temperature conductivity ($\sigma_{300\mathrm{K}}$) for different engineered garnet compositions (across 600–1200 K). Values in parentheses are the experimentally reported $\sigma_{300\mathrm{K}}$.

Composition	**T (K)**	**E_a (meV)**	**D_0 (cm^2/s)**	log D_0	$e^{-E_a/RT}$	σ_{300K} ($mS\,cm^{-1}$)
LLZO	600–1200	401	8.33×10^{-5}	-4.07	1.60×10^{-7}	7.16×10^{-3} (1.62×10^{-3}, 7×10^{-2})[S1,S2]
Al-LLZO	600–1200	231	1.11×10^{-4}	-3.94	1.20×10^{-4}	4.24 (0.4,[S3] 0.25)[S4]
Ga-LLZO	600–1200	210	9.04×10^{-5}	-4.04	2.77×10^{-4}	7.81 (1.42–6.32)[S4,S5]
Al-F4-LLZO	600–800	323	2.25×10^{-4}	-3.64	3.30×10^{-6}	0.16
	900–1200	182	6.18×10^{-6}	-4.20	8.26×10^{-4}	22.3
Al-F3-LLZO	600–800	328	5.64×10^{-4}	-3.24	2.70×10^{-6}	0.353
	900–1200	179	5.60×10^{-5}	-4.25	9.20×10^{-4}	23.4
F3-LLZO	600–1200	201	1.32×10^{-4}	-3.87	3.90×10^{-4}	16.2
$Li_{6.75}La_3Zr_2O_{12}$	600–1200	151	3.31×10^{-5}	-4.48	2.70×10^{-3}	30

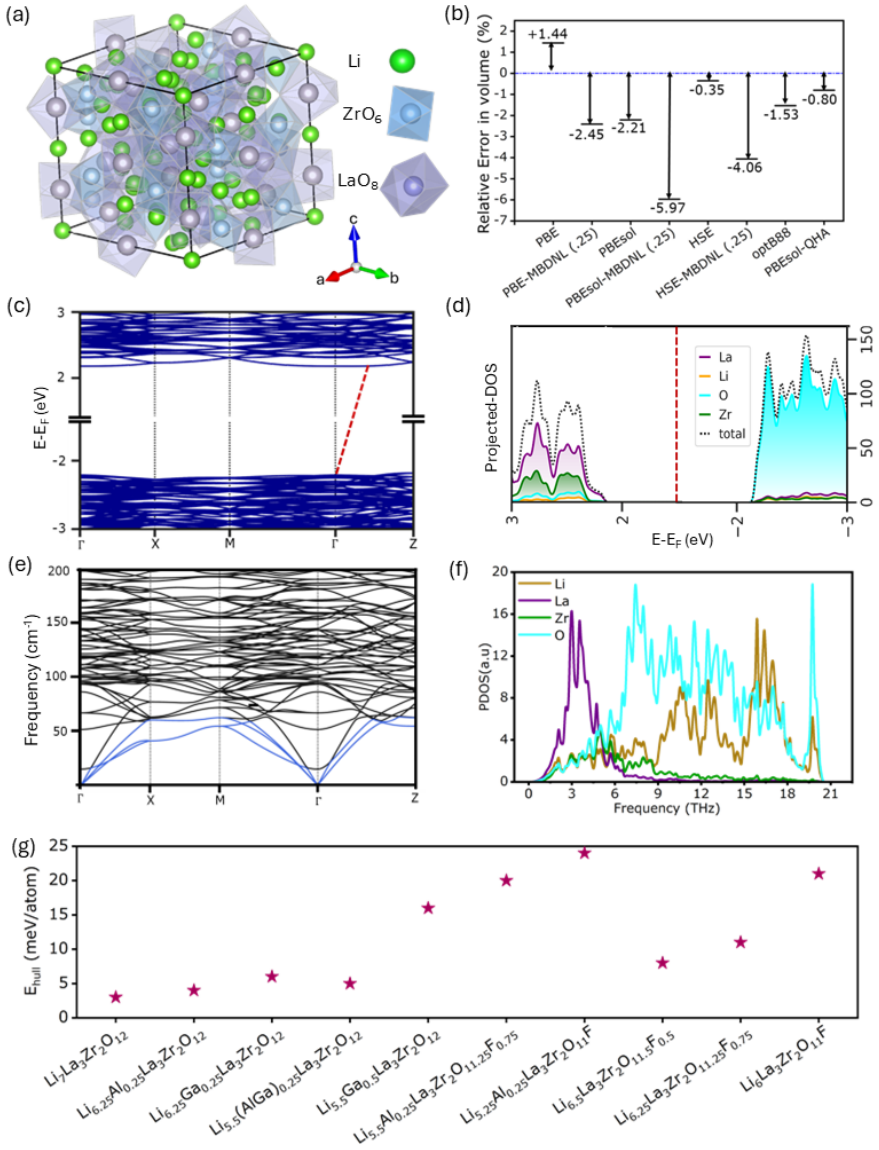

Figure S1: (a) Optimized LLZO structure: Green spheres denote Li atoms; blue and grey polyhedra represent Zr and La, respectively. Framework oxygens are omitted for clarity. (b) Functional benchmarking: Relative error (%) in unit cell volume compared to experimental values. (c) Electronic band structure of tetragonal LLZO using PBEsol, with the indirect band gap marked by a red dashed line and Fermi level set at $E_{\mathrm{F}} = 0$. (d) Element-projected density of states (PDOS) showing contributions from Li, La, Zr, and O atoms. (e) Phonon dispersion spectrum computed with PBEsol, indicating dynamical stability (acoustic modes in blue, optical modes in black). (f) Species-projected phonon density of states (PhDOS). (g) Plot of the energy above the convex hull, E_{hull}(meV/atom), for $Li_7La_3Zr_2O_{12}$ (LLZO) and engineered LLZO variants, computed using the PBEsol functional.

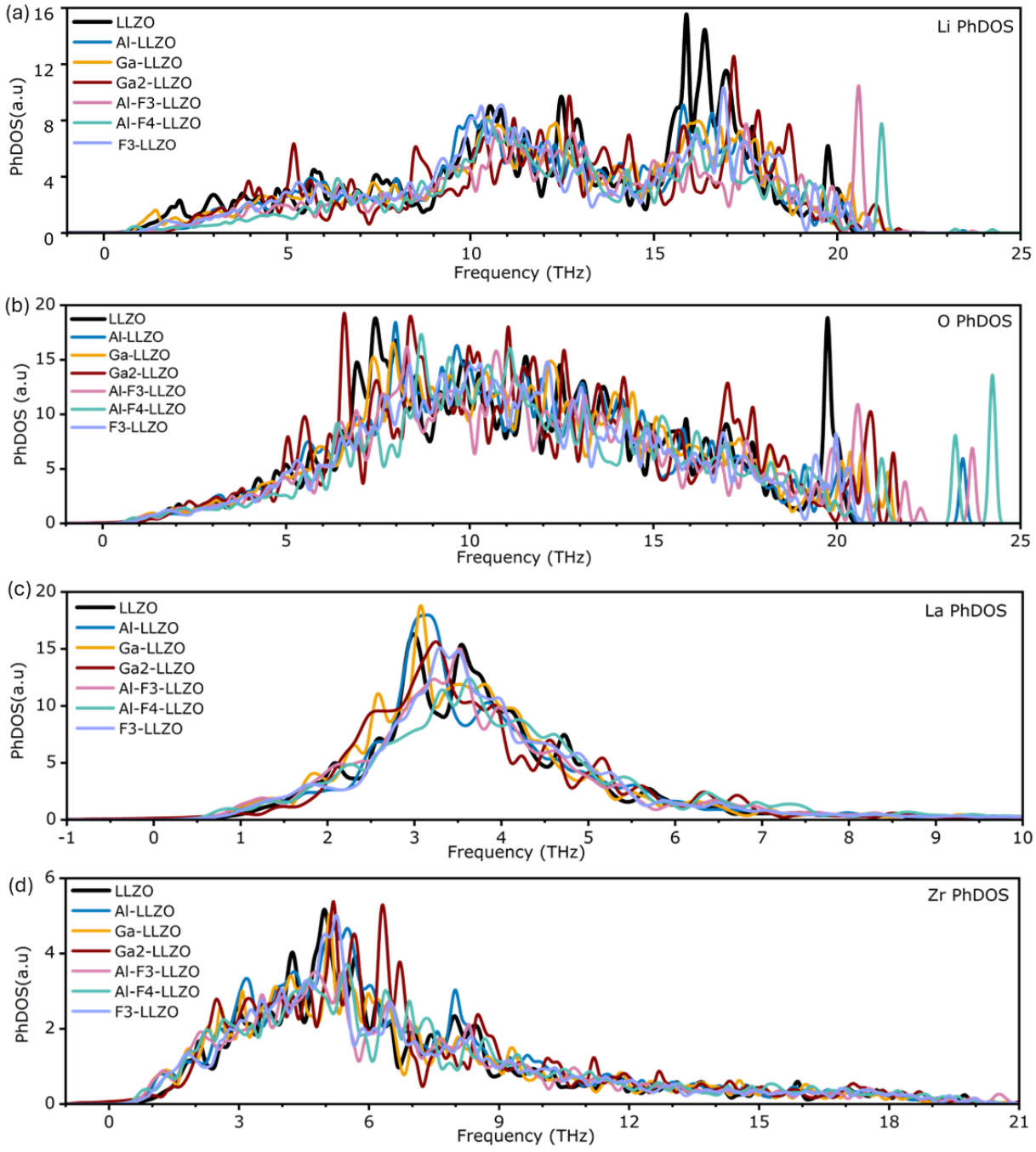

Figure S2: Species-projected phonon density of states (PhDOS) for LLZO and engineered variants. Each panel highlights the vibrational contributions of the respective species across different compositions: (a) Li atoms, (b) O atoms, (c) La atoms, and (d) Zr atoms.

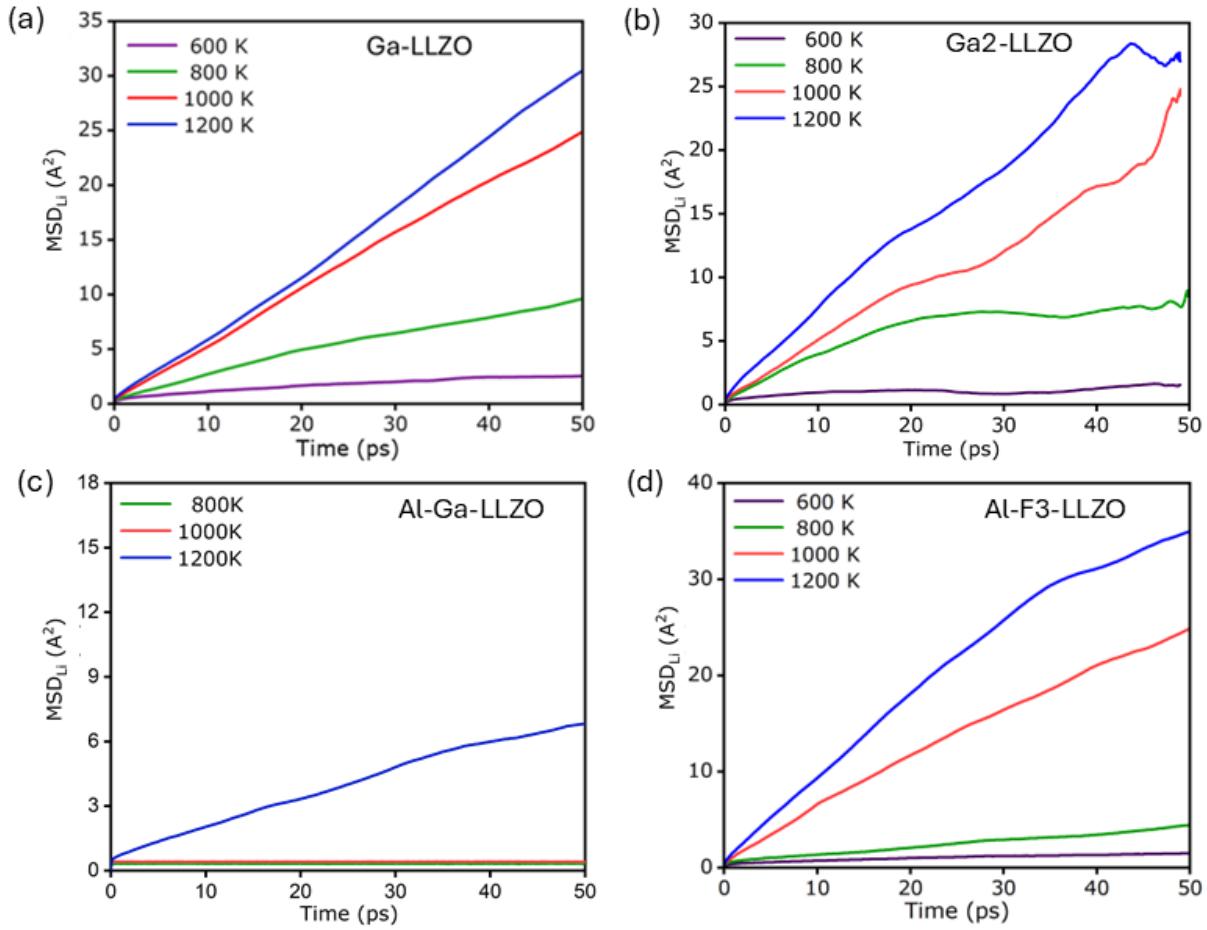

Figure S3: Mean square displacement (MSD) plots of Li-ions at temperatures from 600 to 1200 K for: (a) Ga-LLZO, (b) Ga-rich LLZO (Ga2-LLZO), (c) Al-Ga-LLZO, and (d) Al-F3-LLZO.

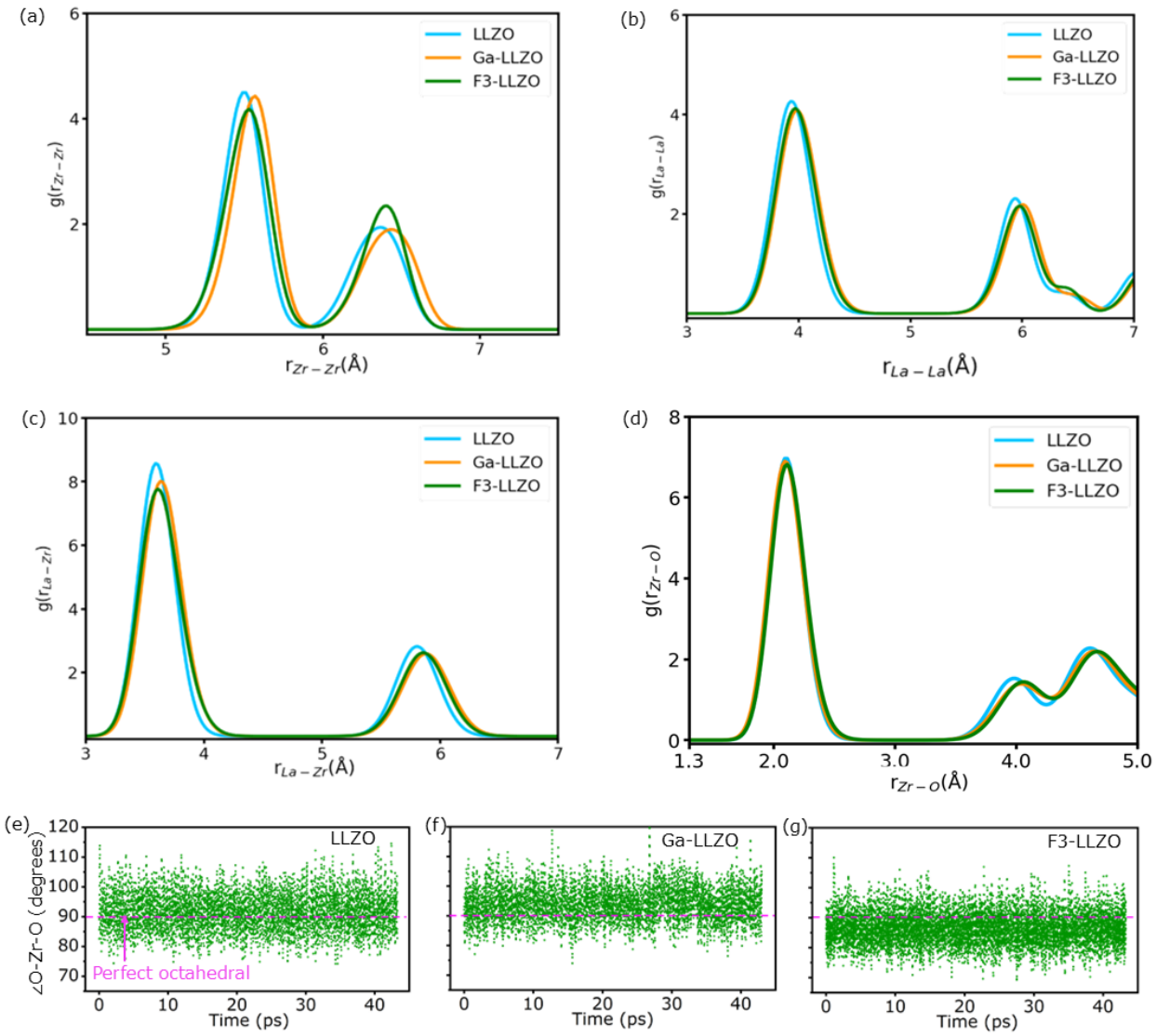

Figure S4: Radial distribution function (RDF) plots from AIMD simulations at 800 K for LLZO, Ga-LLZO, and F3-LLZO: (a) Zr–Zr RDF, (b) La–La RDF, (c) La–Zr RDF and (d) Zr-O RDF. Angular distributions from AIMD simulations at 800 K: (e–g) O–Zr–O bond angles for pristine LLZO, Ga-LLZO, and F3-LLZO, respectively.

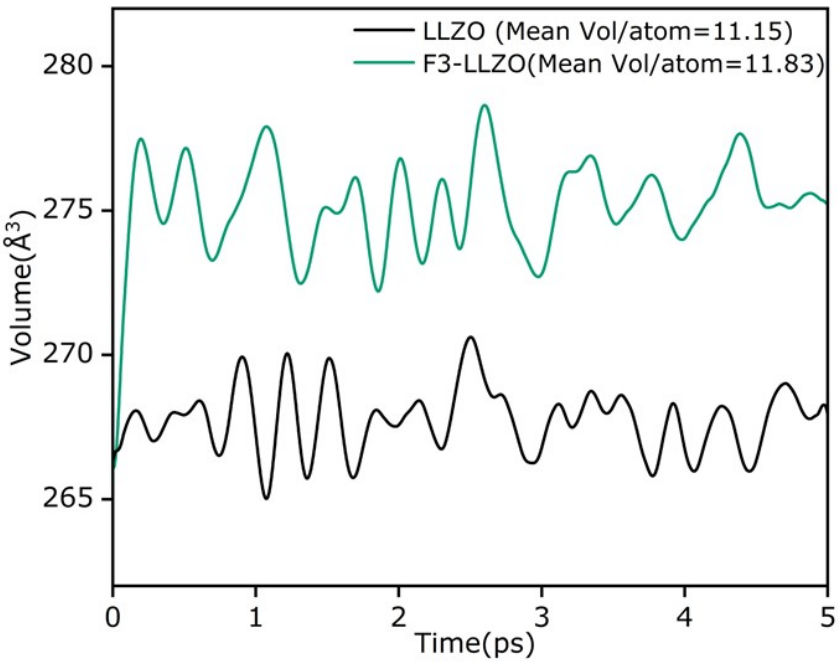

Figure S5: (a) Time evolution of volume per formula unit at 300 K from 5 ps AIMD simulations in the NPT ensemble.

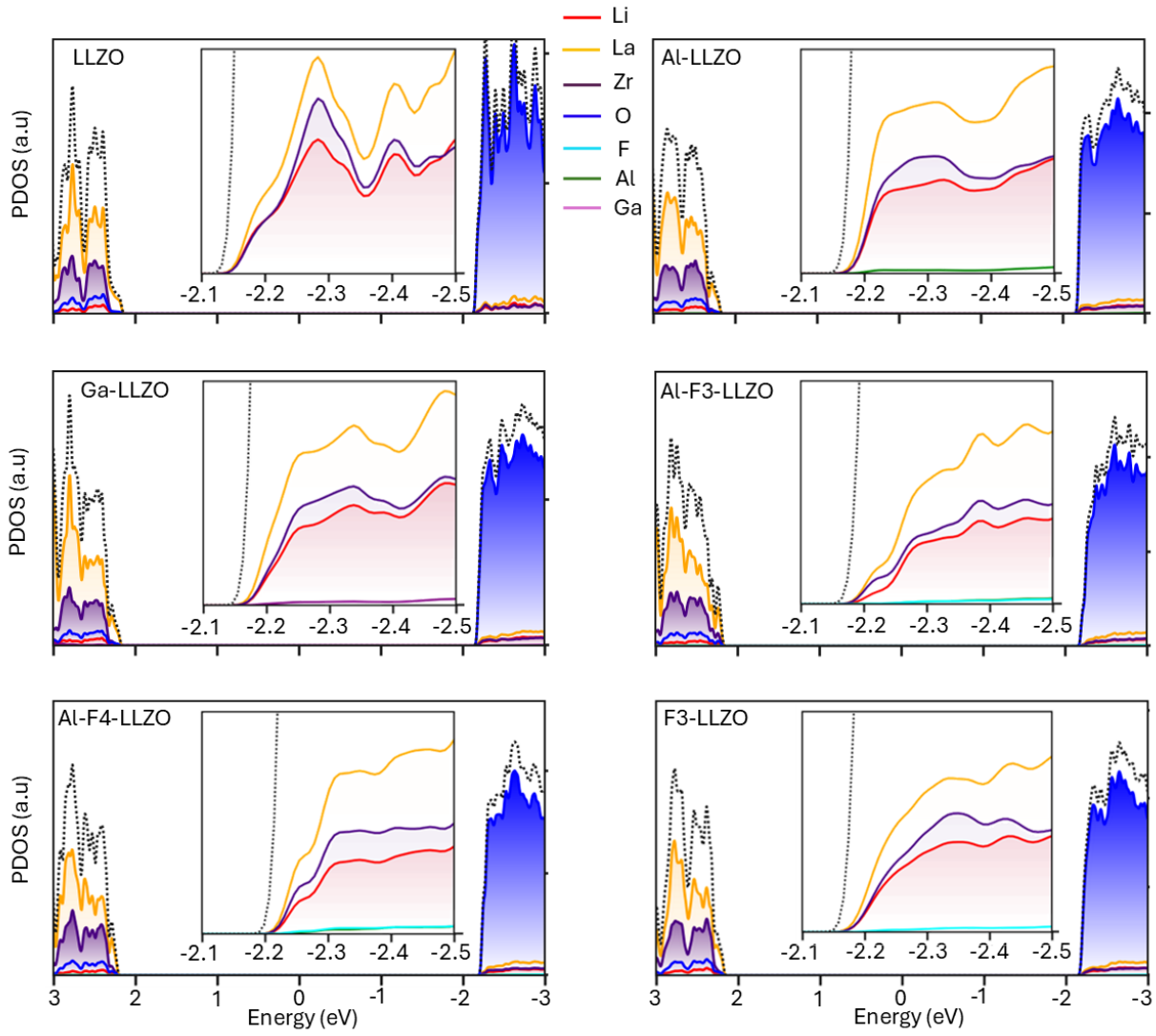

Figure S6: Element-projected density of states (PDOS) for pristine and engineered LLZO structures, showing contributions from individual elements. The Fermi level is set to zero ($E_F = 0$).

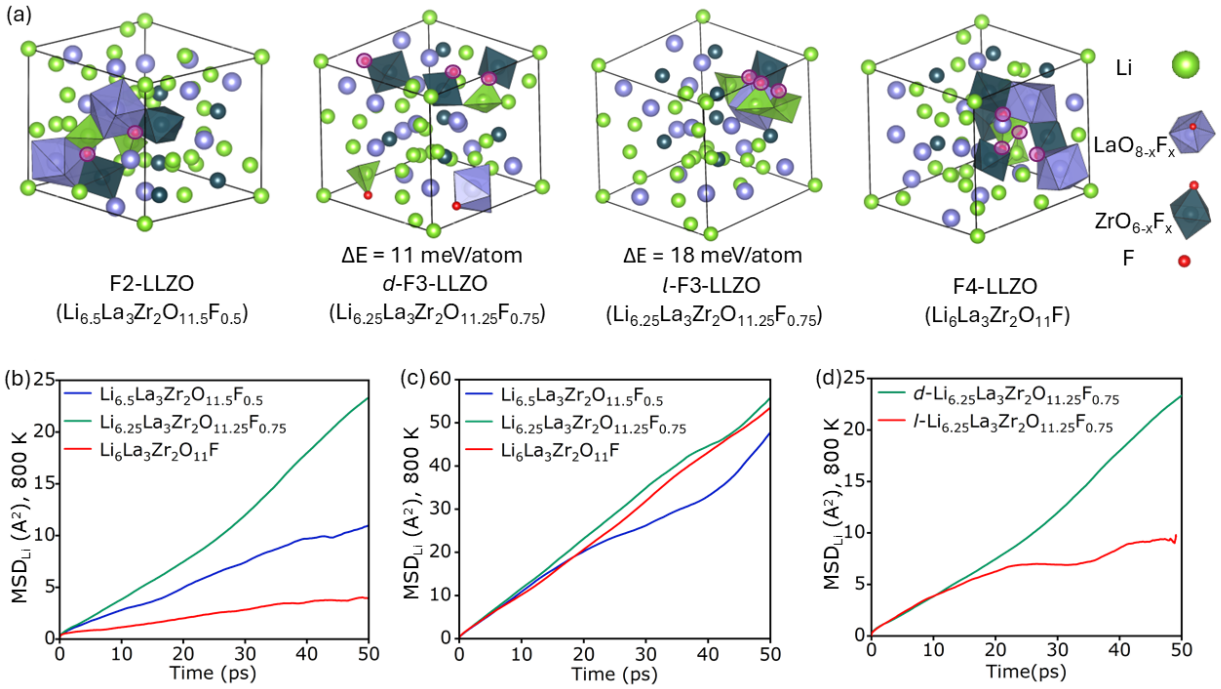

System	$\mathbf{Li_{6.5}La_3Zr_2O_{11.5}F_{0.5}}$	d–$\mathbf{Li_{6.25}La_3Zr_2O_{11.25}F_{0.75}}$	l–$\mathbf{Li_{6.25}La_3Zr_2O_{11.25}F_{0.75}}$	$\mathbf{Li_6La_3Zr_2O_{11}F}$
MSD_{800K} (50 ps)	11.0	23.3	9.6	4.0
MSD_{1200K} (50 ps)	47.8	55.8		53.5
$\frac{MSD_{1200K}}{MSD_{800K}}$	4.4	2.4		13.3

Figure S7: **(Top)** (a) Optimized structures of LLZO with varying fluorine content, including both distributed (d-F3-LLZO) and localized (l-F3-LLZO) configurations for $F_{0.75}$, along with their energy above hull values (E_{hull}). (b) Li-ion mean square displacement (MSD) at 800 K for F2-, F3-, and F4-LLZO. (c) Li-ion MSD at 1200 K for the same compositions. (d) MSD comparison at 800 K between d-F3-LLZO and l-F3-LLZO. **(Bottom)** Summary of MSD values at 800 K and 1200 K, along with their ratios.

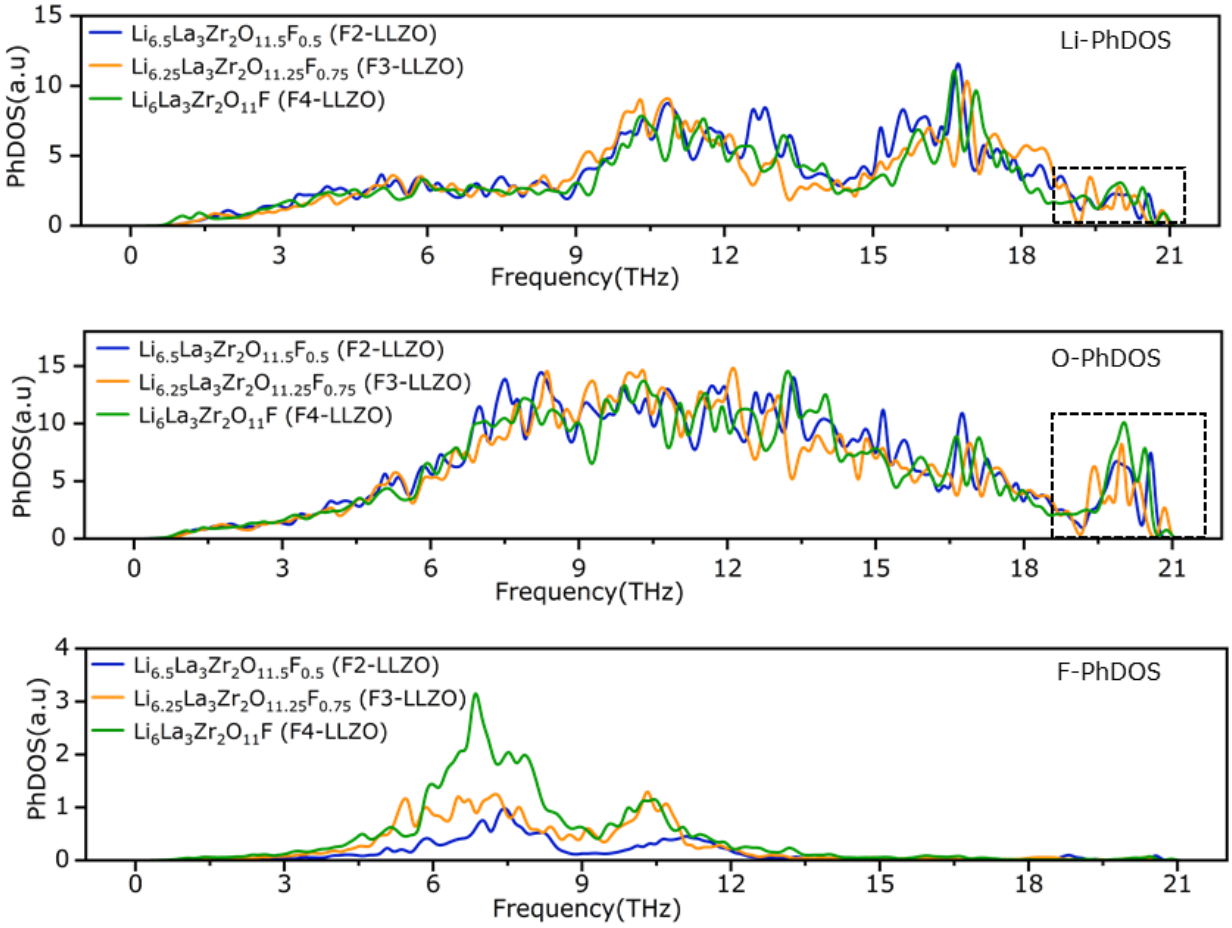

Figure S8: Species-projected phonon density of states (PhDOS) for fluorine-doped LLZO systems: $Li_{6.5}La_3Zr_2O_{11.5}F_{0.5}$ (F2-LLZO), $Li_{6.25}La_3Zr_2O_{11.25}F_{0.75}$ (*d*-F3-LLZO), and $Li_6La_3Zr_2O_{11}F$ (F4-LLZO). (Top) Comparison of Li PhDOS, (Middle) comparison of O PhDOS, and (Bottom) comparison of F PhDOS across the three compositions. The dashed high-frequency region highlights the variation in Li–O and lattice oxygen vibrations as a function of fluorine concentration.

Table S4: Mechanical properties comparison of LLZO and engineered LLZO systems, with bulk modulus (B), Shear modulus (G) and Ductility (Ratio of Bulk modulus and Shear modulus).

System	**B (GPa)**	**G (GPa)**	**B/G**
LLZO	127.12	77.29	1.64
Al-LLZO	124.28	71.28	1.74
Ga-LLZO	126.20	70.19	1.79
Al-F4-LLZO	117.79	69.01	1.70
Al-F3-LLZO	142.10	71.19	1.99
F3-LLZO	155.69	77.72	2.03

References

(S1) Awaka, J.; Kijima, N.; Hayakawa, H.; Akimoto, J. Synthesis and structure analysis of tetragonal Li7La3Zr2O12 with the garnet-related type structure. *Journal of solid state chemistry* **2009**, *182*, 2046–2052.

(S2) Murugan, R.; Thangadurai, V.; Weppner, W.; others Fast lithium ion conduction in garnet-type Li7La3Zr2O12. *ANGEWANDTE CHEMIE-INTERNATIONAL EDITION IN ENGLISH-* **2007**, *46*, 7778.

(S3) El-Shinawi, H.; Paterson, G. W.; MacLaren, D. A.; Cussen, E. J.; Corr, S. A. Low-temperature densification of Al-doped Li 7 La 3 Zr 2 O 12: a reliable and controllable synthesis of fast-ion conducting garnets. *Journal of Materials Chemistry A* **2017**, *5*, 319–329.

(S4) Chen, C.; Sun, Y.; He, L.; Kotobuki, M.; Hanc, E.; Chen, Y.; Zeng, K.; Lu, L. Microstructural and electrochemical properties of Al-and Ga-doped Li7La3Zr2O12 garnet solid electrolytes. *ACS Applied Energy Materials* **2020**, *3*, 4708–4719.

(S5) Jalem, R.; Rushton, M.; Manalastas Jr, W.; Nakayama, M.; Kasuga, T.; Kilner, J. A.;

Grimes, R. W. Effects of gallium doping in garnet-type Li7La3Zr2O12 solid electrolytes. *Chemistry of Materials* **2015**, *27*, 2821–2831.